Journal of Materials Chemistry C

ROYAL SOCIETY OF CHEMISTRY

PAPER

View Article Online
View Journal | View Issue

Cite this: J. Mater. Chem. C, 2020, 8, 1048

Circularly polarized luminescence from semiconductor quantum rods templated by self-assembled cellulose nanocrystals†

Yue Shi,[a] Ziming Zhou,[a] Xiaofei Miao,[b] Yan Jun Liu,[a] Quli Fan,[b] Kai Wang,[a] Dan Luo*[a] and Xiao Wei Sun*[a]

Received 21st October 2019,
Accepted 3rd December 2019

DOI: 10.1039/c9tc05751j

rsc.li/materials-c

Fluorescent semiconductor quantum nanocrystals have received much attention due to their high brightness and color purity. Fabrication of semiconductor quantum nanocrystals with optical activity is of particular interest recently due to the potential applications in the fields of chemistry, pharmacology, biology and physics. Several approaches have been developed to induce circular dichroism and circularly polarized luminescence of semiconductor quantum nanocrystals, but only resulted in very weak signals. Herein, we demonstrate a circularly polarized luminescent solid film by doping CdSe/CdS quantum rods into the self-assembled left-handed helical structure of the earth-abundant and renewable cellulose nanocrystals. The degree of circularly polarized luminescence can be tuned by adjusting the photonic band gap of the helical structure relative to the photoluminescent band. A significant right-handed circularly polarized luminescence has been demonstrated, offering an easy and powerful platform to produce circularly polarized luminescence of semiconductor quantum materials.

Introduction

Semiconductor core–shell quantum nanocrystals (NCs), especially CdSe/CdS type ones, have attracted much attention due to their high brightness, enhanced photoluminescence (PL) quantum yields, good environmental stability and high color purity,[1,2] which offer widespread promising applications in displays,[3,4] lighting,[5] photovoltaics,[6] labelling,[7] and photonic devices.[8] Among different types of quantum NCs, the recently developed NCs with optical activity have drawn particular attention. As a common natural phenomenon, chirality plays an extremely important role in the fields of chemistry, pharmacology, biology and physics.[9] Therefore, quantum NCs with non-zero circular dichroism (CD) and circularly polarized luminescence (CPL) not only attract mechanism explorations,[10,11] but also offer potential applications in chiral recognition,[12] biological sensing,[13] information storage and security devices.[14] In order to induce the optical activity of semiconductor quantum NCs, several approaches have been applied. For example, the NCs with intrinsic dissymmetry of dislocations or defects show non-zero CD;[15,16] the π-conjugated interactions between the chiral ligands and achiral NCs could induce both non-zero CD and CPL;[17,18] and some chiral ligands could drive hierarchical self-assembly of NCs, resulting in helical supraparticle structures and optical activities.[19,20] However, most of these methods not only need tedious synthesis procedures but also give very low chiral signals, where the dissymmetry factors are on the order of 10^{-3}–10^{-4}.[15–20] Besides the above approaches, doping achiral quantum NCs into a chiral supramolecular system has opened up great possibilities for the design and fabrication of functional luminescent materials with optical activity,[21,22] where the chirality of the assembled templates or host matrices can be transferred to the NCs. To achieve the high optical activity of quantum NCs, the self-assembled cholesteric (chiral nematic) liquid crystal (LC) with a one-dimensional (1D) helical structure provides one of the most promising templating matrices.[23]

Cellulose, which can be easily derived from earth-abundant sources such as cotton and wood, is a low-cost, renewable and biocompatible material. When subjected to acid hydrolysis, the cellulose fibers can be extracted into rod-like cellulose nanocrystals (CNCs) with a typical width of 5–10 nm and a length of 50–300 nm.[24,25] The hydrolyzed CNCs after suphuric acid treatment have sulfonate groups on the surfaces, and therefore the fibers show excellent dispersity in water with negative charges.[26] On the other hand, the intrinsic chiral glucose units give them chiral properties.[24] If above a critical concentration,

[a] Department of Electrical and Electronic Engineering, Southern University of Science and Technology, No. 1088, Xueyuan Rd., Xili, Nanshan District, Shenzhen, Guangdong 518055, China. E-mail: luod@sustech.edu.cn, sunxw@sustech.edu.cn
[b] Key Laboratory for Organic Electronics and Information Display & Institute of Advanced Materials, Jiangsu National Synergetic Innovation Center for Advanced Materials, Nanjing University of Posts & Telecommunications, Nanjing 210023, China

† Electronic supplementary information (ESI) available. See DOI: 10.1039/c9tc05751j

the aqueous suspension of CNCs with a high-aspect-ratio shows a left-handed chiral nematic lyotropic LC organization by self-assembling based on Onsager's theory.[27] Moreover, the helical ordering can be preserved upon drying to form a solid chiral film.[28] This chiral film could provide a robust templating matrix compared to the surfactant-based lyotropic[29] or thermotropic LC system[30] and is suitable for large scale production. Taking advantage of this property, the CNCs have been applied as hosts for various nanomaterials.[31–33] In particular, by doping luminescent materials into the self-assembled chiral CNCs, superior CPL signals could be achieved.[34–36] Although semiconductor core–shell quantum NCs have been doped into CNCs and composite luminescent materials have been achieved,[37,38] no optical activity has been reported to the best of our knowledge. Herein, we demonstrate that a significant CPL can be obtained from the semiconductor CdSe/CdS quantum rods (QRs) templated by the CNC helical structure. Our work extends the luminescent materials with optical activity from luminescent dye,[34] upconversional nanoparticles[35] and carbon dots[36] to semiconductor NCs.

Experimental

Synthesis and functionalization of CdSe/CdS QRs

Dot-like CdSe seeds were synthesized by a hot-injection seed growth approach to give red light emission, and then rod-like CdS shells were grown on CdSe cores in a mixture of some alkyl phosphonic acids to passivate the surface defects on CdSe seeds and consequently achieve high PL quantum yields.[39,40] After the reaction, the fabricated CdSe/CdS core/shell QRs were purified three times by adding chloroform and ethanol, and centrifuged at 10 000 rpm for 3 min. The purified QRs were then dispersed into *n*-hexane. In the next step, the ligands of the synthesized CdSe/CdS QRs were exchanged to cysteamine. 270 mg cysteamine (95%, Sigma-Aldrich) and 2.7 ml tetramethylammonium hydroxide solution (25 wt% in H_2O, Sigma-Aldrich) were dissolved into 8.1 ml deionized (DI) water in a vial. Then, 5 ml 1 μM QR in *n*-hexane solution was poured into a vial, followed by 8 hours shaking. Afterwards, most of the QRs were transferred from the oil phase to the water phase. The QRs in water were purified twice by ultrafiltration centrifugation with 8000 rpm for 15 min. At last, these purified QRs with cysteamine ligands were dispersed into DI water and diluted to 1 μM for further use.

Synthesis of CNCs

15 g commercial cellulose filter papers (Whatman) were hydrolyzed in 200 g of 64 wt% sulphuric acid solution under vigorous stirring at 45 °C in a water batch for 2 hours. The pulp was then diluted ten times with DI water to stop hydrolysis at room temperature, followed by centrifugation three times with DI water to remove the amorphous cellulose regions and excess sulfuric acid. The centrifugation was performed at 9000 rpm for 10 min for the first and second times, and at 15 000 rpm for 30 min for the third time (Cence H2500R-2). The resulting sediment was then dialyzed using dialysis tubes (Viskase MWCO 8000–14 000) in DI water for 3 days. Afterwards, the thick slurry was neutralized by using sodium hydroxide to pH = 7, and diluted to the desired concentration for further use. For transmission electron microscopy (TEM) characterization (Hitachi HT7700), a copper grid with an ultra-thin carbon film was dipped into a 0.35 wt% CNC suspension, and then the grid was dried under ambient conditions without further stain.

Preparation of CNC solid films

7 ml of the 3.5 wt% CNC aqueous suspension was sonicated at full power (250 W, Kunshan Ultrasonic Instruments KQ-250DE) in an ice-water bath at certain time periods. Then the suspension was poured into a polystyrene Petri dish (35 mm). After slow water evaporation of 3–5 days under ambient conditions, a solid film was obtained at the bottom and it could be peeled off for further characterization. The thickness of the solid film is about 70 μm. Scanning electron microscopy (SEM, Zeiss Gemini 300) was used for characterizing the microstructure of the dried film, which was peeled to expose the internal structure and then coated with 5 nm Pt (Quorum Q150TES).

Preparation of CNC–QR composite samples

The 3.5 wt% CNC aqueous suspensions were sonicated in an ice-water bath at different time periods prior to QR mixing. Then 7 ml of CNC suspension and 1 μM cysteamine-capped CdSe/CdS QR aqueous suspension were mixed at a desired volume ratio, followed by 10 min sonication and 90 min stirring at room temperature before pouring into a polystyrene Petri dish for drying. The TEM and SEM characterization of the QR–CNC composite materials followed the same procedures as the pure CNC case. To extend the lifetime of the photoluminescent composite material, the dried solid film could be sealed between two glass substrates using UV glue in a N_2 environment.

Results and discussion

Fig. 1a shows the extracted rod-like CNCs with a high-aspect-ratio visualized by TEM. In dilute aqueous suspension, the CNCs are randomly oriented in the isotropic phase and no birefringence is observed under polarized optical microscopy (POM). When the aqueous concentration reaches above 3.5 wt%, the CNCs start to form the cholesteric LC phase with typical fingerprint textures as shown in Fig. 1b, where the periodic spacing between the two adjacent dark lines is the half-helical pitch. During the water evaporation process, the isolated cholesteric droplets grow in size and merge to form a large area cholesteric LC texture. The fingerprint periodicity decreases and the birefringence increases with a higher CNC concentration, indicating that the helical pitch shrinks (Fig. 1b and c). After slow water evaporation under ambient conditions, the CNC suspension is dried to form a solid film. The SEM images show that the film has a periodic structure with counterclockwise twisting, indicating a left-handed helical morphology (Fig. 1d). The helical pitches of the dried films are on the order of few hundred nanometers, and therefore the chiral solid films show iridescent colors due to the selective

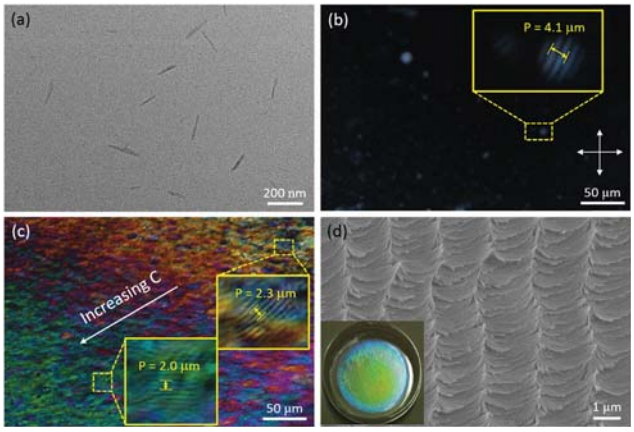

Fig. 1 Characterization of CNCs. (a) TEM images of fibrillary CNCs. POM images of (b) cholesteric droplets surrounded by the isotropic phase formed in a CNC suspension and (c) cholesteric texture with the increasing concentration during water evaporation. The glass cell is 150 μm-thick without any surface treatment. The pitch measurements are shown in the enlarged views (5.2 times) in the insets. (d) SEM image of a CNC solid film showing a left-handed periodic chiral arrangement of CNCs. Inset: The dried CNC film in a Petri dish with iridescent color.

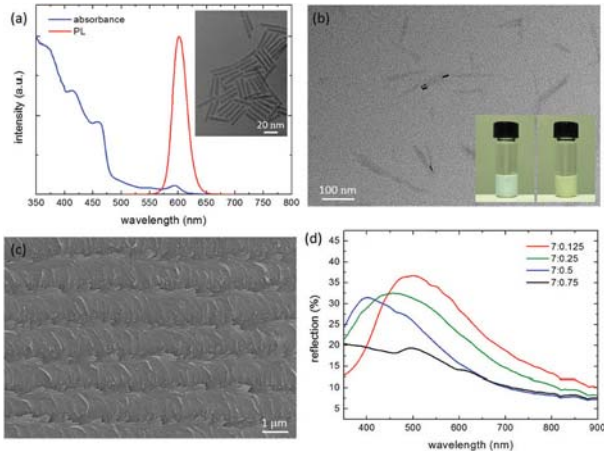

Fig. 2 Characterization of CdSe/CdS QRs and the composite mixture with CNCs. (a) The normalized absorbance and PL spectra of QRs. Inset: TEM image of QRs. (b) TEM image of the CNC–QR composite material at the volume ratios of 7 : 0.25. The gray fibers are CNCs, and the black rods are the bound QRs. Inset: The CNC suspensions without (left) and with (right) QRs. (c) SEM image of the CNC–QR composite solid film. (d) Reflection spectra of the CNC–QR composite films at different volume ratios of CNCs to QRs.

reflection of visible light[42] (the inset of Fig. 1d). The helical pitch can be tuned by changing the electrostatic repulsions between CNCs, where sonication or electrolyte addition is usually applied prior to film casting.[26,41] In particular, simple sonication could increase the electrostatic repulsion and result in a red-shift of the iridescent colors, which is applied in our experiments (Fig. S1, ESI†).

The semiconductor CdSe/CdS core–shell QRs were first synthesized by a hot-injection seed growth approach in the organic phase[39,40] and then ligand-changed with cysteamine to obtain cysteamine-capped CdSe/CdS QRs in the aqueous phase. The synthesized QRs are 5 nm in width and 30 nm in length as illustrated by TEM (Tecnai F30) in Fig. 2a. The QRs show strong absorbance in the ultraviolet (UV) and blue region, and emit red fluorescent luminescence at 602 nm. The ligand cysteamine is chosen because it renders the capped QRs water soluble and the short ligand length gives a small lateral size of QRs. On the other hand, the cysteamine has cationic ammonium peripheral end groups in aqueous solution, so that the QRs could be adsorbed onto CNCs by electrostatic interactions without disturbing their intrinsic structure. The TEM image of the CNC–QR composite material in Fig. 2b shows that the QRs are well bound to CNCs, and no dissociative QRs are observed throughout the TEM sample grid. Moreover, the CNC–QR composite suspensions are visually clear after mixing over months without macroscopic aggregations, indicating that the electrostatic interaction between cationic QRs and anionic CNCs also helps to increase the stability of QRs and avoid their aggregations. After being dried for 3–5 days under ambient conditions, the composite suspensions are dried to form a solid film with iridescent colors. The dried solid film shows a typical left-handed helical morphology as illustrated by SEM (Fig. 2c), the same as the one formed by pure CNCs (Fig. 1d). Therefore, the cysteamine-capped CdSe/CdS QRs are well bound to CNCs without disturbing their intrinsic chiral structure and self-assembling properties, where the preparation and self-assembling process of the CNC–QR composite material is illustrated in Scheme 1.

The CNC–QR composite suspensions are prepared with 3.5 wt% CNCs and 1 μM QRs in aqueous suspensions at volume ratios of 7 : 0.125, 7 : 0.25, 7 : 0.5 and 7 : 0.75 with the same sonication time of 1 h. The zeta potentials are measured to be – 39.8 mV, −35.7 mV, −29.5 mV and −22.15 mV, respectively (Brookhaven ZetaPALS), which are as expected since more

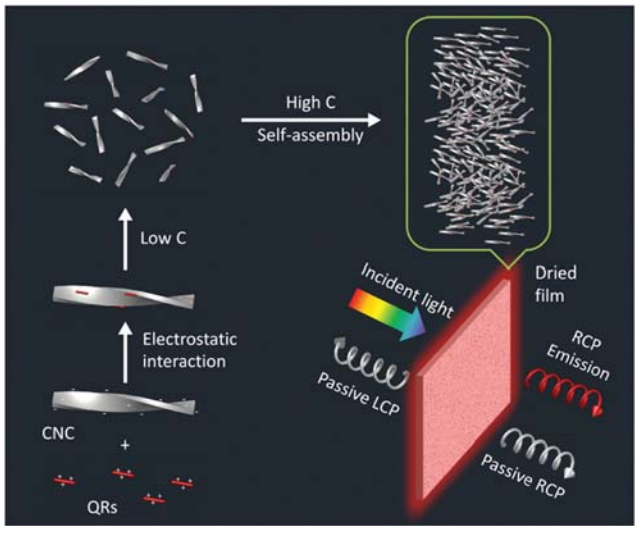

Scheme 1 Schematic illustration of the self-assembled CNC–QR composite solid film. The QRs bind onto fibrillary CNCs by electrostatic interactions in aqueous suspension. When above a critical concentration, the CNCs are self-assembled to form the lyotropic cholesteric LC phase with a left-handed helical structure. The helical ordering is preserved upon drying to form a solid chiral film. The composite chiral film enables RCP emission due to the forbidden propagation of LCP light.

cationic QRs could reduce the electrostatic repulsion between the anionic CNCs. The four CNC–QR composite suspensions are all visually clear after mixing over months, consistent with the measured zeta potentials where the absolute values are high enough to avoid aggregations. The iridescent colors of the dried solid films are blue-shifted with the increasing amount of QRs as a result of their reduced repulsions, which are confirmed by the reflection spectrum measurements in Fig. 2d (Craic Tech.). However, for the composite film with a high QR concentration, the reflection is suppressed in the UV region as shown for the 7 : 0.75 film due to its high absorbance. The spectrum dips at 460 nm and 600 nm also come from the QR absorbance. This effect still appears for the 7 : 0.5 composite film, where the spectrum dip at 460 nm could be noticed. Therefore, to explore the optical activity of CNC–QR composite films, a 7 : 0.25 volume ratio is chosen for the following experiments to ensure high PL intensity while the iridescent colors could be hardly influenced by the intrinsic reddish color of QRs.

To compare the optical activity of CNC–QR composite films, the films were prepared with iridescent colors across a wide spectral range. With the total sonication time varying from 40 min to 90 min, the film iridescent colors changed from UV to red (Fig. 3a and b). Here, a longer total sonication time is applied to the composite suspensions compared to pure CNCs, since the electrostatic repulsions between composite fibers are reduced due to the QR introduction. When viewed under UV light, these composite films appear to have similar red PL brightness due to the same QR loading (Fig. 3c). The reflection spectra of these composite films are measured to be centered at 386 nm, 440 nm, 530 nm and 600 nm, respectively (Fig. 4a), consistent with their iridescent colors. The iridescent color of the chiral solid film comes from the photonic band gap (PBG) of the 1D chiral photonic crystal with a periodic helical structure. Due to the preferential reflection of left circularly polarized (LCP) light, the films show positive CD activity (Fig. 4b), where CD is the extinction difference between the LCP and right circularly polarized (RCP) light measured by a Chirascan spectrometer (Applied Photophysics). The CD signals of these composite films are higher than 7000 mdeg which have exceeded the saturation value of the instrument. This value is much stronger compared to that produced by other methods.[15–20] To confirm the CD origin of the chiral solid film, the CD signal of CNC–QR composite suspensions was also measured. The CD spectra of different CNC–QR volume ratios overlap well with those of the pure CNCs suspension (the inset of Fig. 4b), indicating that the interaction between QRs and CNCs does not induce any additional CD signal. This is probably because the fact that the lateral sizes of QRs and fibrillary CNCs are mismatched and the QRs on CNCs are too dilute to produce any dipole coupling effect.[43] On the other hand, although the CD spectra are saturated, the peak positions are still recognizable, which are consistent with the corresponding reflection peaks as shown in Fig. 4a. Therefore, the positive CD signals at the corresponding reflection bands are due to the 1D PBG of the left-handed self-assembling structure of the CNC–QR composite films.

Besides strong CD, the combination of photoluminescent QRs and tunable PBGs of the CNC films allows the manipulation of the PL optical activity. The CPL spectra, which are the PL difference between LCP and RCP light, were measured by a JASCO CPL-300 spectrometer. The luminescence dissymmetry factor of CPL is defined as $g_{lum} = 2(I_L - I_R)/(I_L + I_R)$, where I_L and I_R are the emission intensity of LCP and RCP light, respectively.[44] The g_{lum} value ranges from +2 for an ideal LCP light to −2 for an ideal RCP light, while $g_{lum} = 0$ corresponds to no chiral luminescence. As shown in Fig. 4c and d, the measurements indicate that when the QR's PL band is away from the composite film's PBG, the CPL signal is weak. As the two bands approach, the signal gets stronger. When the QR's PL band is superimposed with the film's PBG, the optical activity of the CNC–QR composite film becomes the strongest, where the CPL reaches −5900 mdeg and the

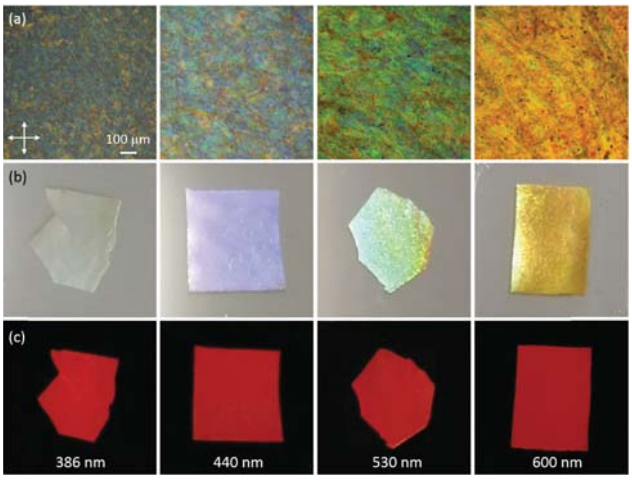

Fig. 3 The CNC–QR composite films with iridescent colors varing from UV to red. (a) Reflective POM images of the CNC–QR composite films. (b) The films under natural light showing pale blue, blue, green and yellow-red iridescent colors from left to right. (c) Corresponding luminescent photos under 365 nm UV light. The films are marked as the center reflective wavelength as 386 nm, 440 nm, 530 nm and 600 nm, respectively.

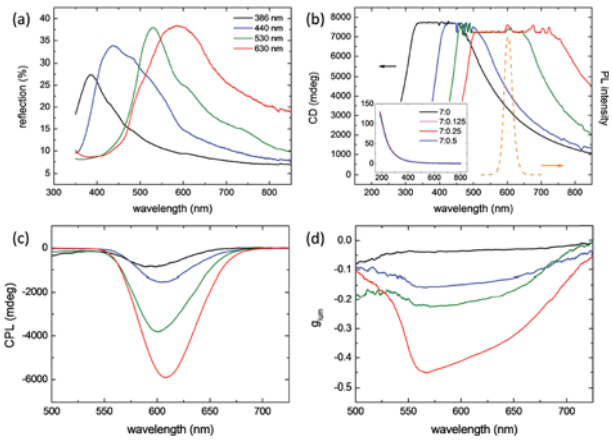

Fig. 4 Optical characterization of the CNC–QR composite films. (a) Reflection spectra. (b) CD spectra. The dashed orange curve is the PL spectrum of QRs. Inset: CD spectra of the composite suspensions with different volume ratios of CNCs to QRs. (c) CPL spectra. (d) g_{lum} spectra. The curves are labelled by the center reflective wavelength.

dissymmetry factor g_{lum} is −0.45, giving a high contrast of LCP and RCP light. Since no additional CD signal is induced from dipole coupling, the CPL originates from the microscopic helical superstructure rather than molecular chirality transfer. Basically, linearly polarized PL is locally emitted by each QR, which can be considered as a combination of LCP and RCP light. When the QR's PL band overlaps with the film's PBG, the fluorescence quantum yield of LCP emission is reduced due to the forbidden propagation of CPL with the same helicity of the film,[45] leaving only RCP emission passing through. No linear polarization artefacts exist in the PL of the composite film, which has been demonstrated in Fig. S2 (ESI†). Therefore, the CNC–QR composite films with left-handed chiral organization could transform the spontaneous emission of QRs within PBG to RCP light, and the process is illustrated in Scheme 1. The non-ideal CPL with g_{lum} = −0.45 is probably due to the non-uniform helical pitches as a result of CNC polydispersity and some off-normal helical axis directions that exist in the self-assembled structures as a result of the non-uniform surface strain during the water evaporation process. Although the CPL strength is not ideal, the luminescence dissymmetry factor g_{lum} = −0.45 is already much significant compared to that induced by other methods, which are on the order of 10^{-3}–10^{-4}.[15–20] Moreover, the preparation procedure of the composite films is simple, together with the superior CPL signal, and the chiral composite film is attractive for developing optical devices with optical activity based on semiconductor NCs.

Conclusions

Circularly polarized luminescent semiconductor CdSe/CdS solid films are achieved by incorporating QRs into a cellulose nanocrystal template with a 1D left-handed helical structure. By adjusting the electrostatic repulsion of the composite material in aqueous suspension, the photonic band gap of the dried helical structure can be tuned from the UV to infrared region, enabling the composite solid film to exhibit adjustable circularly polarized luminescence strength. The superior circularly polarized luminescence with g_{lum} = −0.45 is achieved when the photonic band gap of the cholesteric LC template is overlapped with the photoluminescence band. Therefore, the earth-abundant and renewable cellulose nanocrystals offer an easy and powerful platform to produce photonic bandgap-based circularly polarized luminescence, and our work extends the luminescent material from luminescent dyes, upconversional nanoparticles, and carbon dots to semiconductor quantum nanocrystals.

Conflicts of interest

There are no conflicts to declare.

Acknowledgements

The authors acknowledge the Material Characterization and Preparation Center of Southern University of Science and Technology. This work was supported by the National Natural Science Foundation of China (NSFC) (61875081) and the Shenzhen Science and Technology Innovation Council (JCYJ20180305180611745, JCYJ20180305180700747, JCYJ20160301113356947 and JSGG20170823160757004).

References

1 D. V. Talapin, R. Koeppe, S. Gözinger, A. Kornowski, J. M. Lupton, A. L. Rogach, O. Benson, J. Feldmann and H. Weller, *Nano Lett.*, 2003, **3**, 1677.
2 I. Coropceanu, A. Rossinelli, J. R. Caram, F. S. Freyria and M. G. Bawendi, *ACS Nano*, 2016, **10**, 3295.
3 T. Du, J. Schneider, A. K. Srivastava, A. S. Susha, V. G. Chigrinov, H. S. Kwok and A. L. Rogach, *ACS Nano*, 2015, **9**, 11049.
4 W. Zhang, J. Schneider, V. G. Chigrinov, H. S. Kwok, A. L. Rogach and A. K. Srivastava, *Adv. Opt. Mater.*, 2018, **6**, 1800250.
5 S. Coe, W.-K. Woo, M. Bawendi and V. Bulović, *Nature*, 2002, **420**, 800.
6 A. J. Nozik, M. C. Beard, J. M. Luther, M. Law, R. J. Ellingson and J. C. Johnson, *Chem. Rev.*, 2010, **110**, 6873.
7 M. Bruchez Jr., M. Moronne, P. Gin, S. Weiss and A. P. Alivisatos, *Science*, 1998, **281**, 2013.
8 J. Schneider, W. Zhang, A. K. Srivastava, V. G. Chigrinov, H.-S. Kwok and A. L. Rogach, *Nano Lett.*, 2017, **17**, 3133.
9 G. H. Wagnière, *On chirality and the universal asymmetry: reflections on image and mirror image*, Wiley-VCH, New York, 2007.
10 A. Ben Moshe, D. Szwarcman and G. Markovich, *ACS Nano*, 2011, **5**, 9034.
11 A. Ben-Moshe, A. Teitelboim, D. Oron and G. Markovich, *Nano Lett.*, 2016, **16**, 7467.
12 A. Kühnle, T. R. Linderoth, B. Hammer and F. Besenbacher, *Nature*, 2002, **415**, 891.
13 Y. Xia, Y. Zhou and Z. Tang, *Nanoscale*, 2011, **3**, 1374.
14 G. R. Meseck, A. S. Terpstra and M. J. MacLachlan, *Curr. Opin. Colloid Interface Sci.*, 2017, **29**, 9.
15 M. V. Mukhina, V. G. Maslov, A. V. Baranov, A. V. Fedorov, A. O. Orlova, F. Purcell-Milton, J. Govan and Y. K. Gun'ko, *Nano Lett.*, 2015, **15**, 2844.
16 A. S. Baimuratov, I. D. Rukhlenko, Y. K. Gun'ko, A. V. Baranov and A. V. Fedorov, *Nano Lett.*, 2015, **15**, 1710.
17 U. Tohgha, K. K. Deol, A. G. Porter, S. G. Bartko, J. K. Choi, B. M. Leonard, K. Varga, J. Kubelka, G. Muller and M. Balaz, *ACS Nano*, 2013, **7**, 11094.
18 J. Cheng, J. Hao, H. Liu, J. Li, J. Li, X. Zhu, X. Lin, K. Wang and T. He, *ACS Nano*, 2018, **12**, 5341.
19 E. D. Sone, E. R. Zubarev and S. I. Stupp, *Small*, 2005, **1**, 694.
20 Y. Zhou, R. L. Marson, G. van Anders, J. Zhu, G. Ma, P. Ercius, K. Sun, B. Yeom, S. C. Glotzer and N. A. Kotov, *ACS Nano*, 2016, **10**, 3248.
21 J. Zhang, W. Feng, H. Zhang, Z. Wang, H. A. Calcaterra, B. Yeom, P. A. Hu and N. A. Kotov, *Nat. Commun.*, 2016, **7**, 10701.
22 J. Han, J. You, X. Li, P. Duan and M. Liu, *Adv. Mater.*, 2017, **29**, 1606503.
23 H. K. Bisoyi, T. J. Bunning and Q. Li, *Adv. Mater.*, 2018, **30**, 1706512.

24 J.-F. Revol, H. Bradford, J. Giasson, R. H. Marchessault and D. G. Gray, *Int. J. Biol. Macromol.*, 1992, **14**, 170.
25 D. Bondeson, A. Mathew and K. Oksman, *Cellulose*, 2006, **13**, 171.
26 X. M. Dong and D. G. Gray, *Langmuir*, 1997, **13**, 2404.
27 L. Onsager, *Ann. N. Y. Acad. Sci.*, 1949, **51**, 627.
28 K. E. Shopsowitz, H. Qi, W. Y. Hamad and M. J. MacLachlan, *Nature*, 2010, **468**, 422.
29 Q. Liu, Y. Cui, D. Gardner, X. Li, S. He and I. I. Smalyukh, *Nano Lett.*, 2010, **10**, 1347.
30 Q. Liu, Y. Ye and I. I. Smalyukh, *Nano Lett.*, 2014, **14**, 4071.
31 A. Querejeta-Fernández, G. Chauve, M. Methot, J. Bouchard and E. Kumacheva, *J. Am. Chem. Soc.*, 2014, **136**, 4788.
32 G. Chu, X. Wang, T. Chen, J. Gao, F. Gai, Y. Wang and Y. Xu, *ACS Appl. Mater. Interfaces*, 2015, **7**, 11863.
33 H. Thérien-Aubin, A. Lukach, N. Pitch and E. Kumacheva, *Angew. Chem., Int. Ed.*, 2015, **54**, 5618.
34 H. Zheng, W. Li, W. Li, X. Wang, Z. Tang, S. X.-A. Zhang and Y. Xu, *Adv. Mater.*, 2018, **30**, 1705948.
35 G. Chu, X. Wang, T. Chen, W. Xu, Y. Wang, H. Song and Y. Xu, *J. Mater. Chem. C*, 2015, **3**, 3384.
36 H. Zheng, B. Ju, X. Wang, W. Wang, M. Li, Z. Tang, S. X.-A. Zhang and Y. Yu, *Adv. Opt. Mater.*, 2018, **6**, 1801246.
37 S.-H. Hwang, C. N. Moorefield, P. Wang, K.-U. Jeong, S. Z. D. Cheng, K. K. Kotta and G. R. Newkome, *Chem. Commun.*, 2006, 3495.
38 C. Chang, J. Peng, L. Zhang and D.-W. Pang, *J. Mater. Chem.*, 2009, **19**, 7771.
39 Z. Zhou, K. Wang, Z. Zhang, C. Zhang, H. Liu, Y. Zhang, Z. Wen, S. Li, J. Hao, B. Xu, S. J. Pennycook, K. L. Teo and X. W. Sun, *IEEE Photonics J.*, 2019, **11**, 2200211.
40 F. Di Stasio, J. Q. Grim, V. Lesnyak, P. Rastogi, L. Manna, I. Moreels and R. Krahne, *Small*, 2015, **11**, 1328.
41 S. Beck, J. Bouchard and R. Berry, *Biomacromolecules*, 2011, **12**, 167.
42 H. L. D. Vries, *Acta Crystallogr.*, 1951, **4**, 219.
43 J. Majoinen, J. Hassinen, J. S. Haataja, H. T. Rekola, E. Kontturi, M. A. Kostiainen, R. H. A. Ras, P. Törmä and O. Ikkala, *Adv. Mater.*, 2016, **28**, 5262.
44 N. Berova, K. Nakanishi and R. W. Woody, *Circular dichroism: principles and applications*, Wiley-VCH, New York, 2000.
45 F. Fleischhaker and R. Zentel, *Chem. Mater.*, 2005, **17**, 1346.